Heliyon 10 (2024) e30503

Contents lists available at ScienceDirect

Heliyon

journal homepage: www.cell.com/heliyon

Research article

Enhancing the efficacy of letrozole-loaded PEGylated nanoliposomes against breast cancer cells: *In vitro* study

Soraya Shahbazi, Farzaneh Tafvizi *, Vahid Naseh

Department of Biology, Parand Branch, Islamic Azad University, Parand, Iran

ARTICLE INFO

Keywords:
Apoptosis
Breast cancer
Cell cycle
Cytotoxicity
Letrozole
PEGylated liposome

ABSTRACT

Considering its overall impact on human health, letrozole (Let) has been described as having significant efficacy that could be improved by developing drug delivery systems. Considering the side effects of Let, this study aims to encapsulate Let in liposomes and PEGylated liposome nanoparticles (Lipo-Let-PEG) and evaluate the cytotoxic effects on the MCF-7 breast cancer cell line. For this purpose, the Lipo-Let-PEG formulation was designed and characterized by SEM, DLS, and FTIR methods, and the drug release from the optimized formulation and the stability of the optimized Lipo-Let-PEG were measured. Furthermore, the cytotoxicity and apoptotic studies were performed using MTT assay and flow cytometric analysis. According to the experimental data, the vesicle size and EE% were 170.05 ± 4.15 nm and 87.21 ± 1.36 %, respectively. The cumulative release from Lipo-Let-PEG at pH 5.4 and 7.4 was also approximately 60 % and 50 %, respectively. MTT results showed that Lip-Let-PEG produced more drug cytotoxicity than Lip-Let against MCF-7 cancer cells and was more compatible with normal cells. The results of apoptosis and cell cycle arrest using flow cytometry show that Lipo-Let-PEG caused the most significant increase in apoptotic rates and cell cycle arrest in cancer cells compared to other treated groups. In conclusion, Lipo-Let-PEG can be used as an anticancer agent by arresting cell cycle progression and inducing apoptosis, which can be applied in future studies to prevent breast cancer development.

1. Introduction

It is estimated that by 2040, there will be 3,000,000 new cases of Breast cancer and 100,000 deaths worldwide [1]. Although there are many different risk factors for breast cancer, including those related to reproduction, genetics, diet, lifestyle, and the environment, the incidence of the disease typically varies by race, ethnicity, socioeconomic status, location, and other variables [2]. However, there has been a massive and sustained increase in breast cancer burden and deaths worldwide over the past 25 years [3]. One of the most effective anticancer therapies to date is breast cancer therapy with estrogen-targeting drugs. For example, letrozole (Let), a third-generation aromatase inhibitor, is the most commonly used anti-estrogen drug in the treatment of breast cancer [4,5]. Let effectively block the estrogen-producing enzyme aromatase, which inhibits the development of hormone-responsive breast tumors *in vivo*. However, studies have shown that Let may cause specific undesirable side effects in some individuals, including diarrhea, constipation, fever, and fatigue [6]. Considering its overall impact on human health, Let has been described as having significant efficacy that could be improved by developing drug delivery systems [7].

* Corresponding author.
E-mail addresses: farzanehtafvizi54@gmail.com, Farzaneh.Tafvizi@iau.ac.ir (F. Tafvizi).

https://doi.org/10.1016/j.heliyon.2024.e30503
Received 2 March 2024; Received in revised form 23 April 2024; Accepted 29 April 2024
Available online 30 April 2024

Liposomes are a valuable resource for the pharmaceutical industry. They have been widely used as a delivery system for the chemotherapy of cancer, genetic disorders, and many other health problems [8–11]. Bilayer or multilayer lipid vesicles, known as liposomes, completely enclose an aqueous volume with a membrane composed of amphiphilic phospholipids [12]. They consist of phospholipid molecules that can self-assemble into lipid bilayer or multilayer vesicles in an aqueous environment [13]. Liposomes can selectively load drugs by entrapping hydrophilic molecules in the aqueous core and hydrophobic molecules in the lipid bilayer. Compared to systemic drug delivery, liposomes offer several advantages [14]. They can reduce interactions with healthy cells and prevent unwanted drug degradation [15]. This improves drug bioavailability and payload at the target sites [16]. Due to their biocompatibility and biodegradability, these systems are less harmful than other nanoparticles [17,18].

Nevertheless, they have a short serum half-life. This problem can be solved by adding poly-(ethylene glycol) (PEG) to the structure of liposomes to create liposomes with a longer serum half-life. PEGylation increases the hydrophilicity of the entrapped drug and reduces the glomerular filtration rate, thereby prolonging its duration in the bloodstream [19]. Furthermore, PEGylation of nanostructures enhances the tumor-targeting efficacy of chemotherapeutics through improved permeation and retention effects [20,21].

Due to the side effects of Let, this study aims to encapsulate Let in PEGylated liposome nanoparticles (Lipo-Let-PEG) and evaluate their anticancer effects on MCF-7 breast cancer cells. For this purpose, the Lipo-Let-PEG formulation was designed and characterized by SEM, DLS, and FTIR methods, and the drug release from the optimized formulation and the stability of the optimized Lipo-Let-PEG were measured. Furthermore, cytotoxicity and apoptotic studies were performed using 3-[4,5-dimethylthiazole-2-yl]-2,5-diphenyltetrazolium bromide (MTT) assay and flow cytometric analysis.

2. Materials and methods

2.1. Lipo-Let-PEG synthesis

Nanoliposomes were prepared using the thin-layer hydration method. Phosphatidylcholine, cholesterol, and mPEG20000-ALD (Merck, Germany) were dissolved in chloroform in a molar ratio of 65:30:5. The resulting solution was poured into a unique rotary flask and placed under vacuum under specified conditions (60 °C and 120 rpm) until the solvent was evaporated entirely. Then, 10 mL of letrozole solution is poured into the balloon along with 10 mL of phosphate-buffered saline (pH 7.4), and the apparatus is operated again for 1 h at the specified temperature and cycle to form a thin layer on the wall. After this step, the balloon contents were transferred to the falcon and then stored in the refrigerator for the remainder of the assay [22].

2.2. Design experiment

In this study, experimental design, statistical analysis, and validation of experimental results were performed using Design Expert software (version 6.0.10, State-Ease, Inc., Minneapolis, MN). In this study, fifteen experiments were designed using the D-optimal design method. In this design, the three factors, including the ratio of distearoylphosphatidylcholine (DSPC) to cholesterol, sonication time, and drug concentration, were considered as test variables (Table 1), and vesicle size, polydispersity index (PDI) and entrapment efficiency (%EE) were considered as experimental responses (Table 2). The selected variable levels were all chosen based on information from previous studies and preliminary screening tests [22].

2.3. Characterization of Lipo-Let-PEG

Field-emission scanning electron microscopy (FE-SEM, TESCAN MIRA3) was used to analyze the morphology of the nanoparticles. Using a nano/zetasizer (Malvern Instruments, Worcestershire, UK, model Nano ZS), the size of the nanoparticles was also determined using the dynamic light scattering (DLS) technique. Fourier transform infrared spectroscopy (FT-IR) (Bruker Tensor 27, Biotage, Germany) was used to verify the chemical properties of the synthesized nanostructures. In transmission mode, FT-IR spectra were recorded between 4000 and 400 cm^{-1} with a resolution of 4 cm^{-1}.

2.4. Entrapment efficiency (EE%)

The ultrafiltration technique was used to determine the encapsulation efficiency of different samples. Shortly after centrifugation of 0.5 mL Lipo-Let-PEG (20 min, 1000 rpm, 4 °C, Eppendorf® 580R centrifuge, Germany), the sample was washed with PBS (pH 7.4). The concentration of Let in the supernatant of each sample was calculated by measuring the absorbance of the supernatant at the wavelength of the maximum absorbance peak of Let (240 nm). The standard curve for Let prepared was used to determine the concentration. The following equation was used to obtain the percentage of encapsulation efficiency (EE%) [22]:

Table 1
Different levels of experiment variables.

Level	−1	0	+1
A (DSPC: cholesterol, mol ratio)	0.5	1	2
B (Sonication time, min)	3	5	7
C (Drug concentration, μg/mL)	250	500	750

Table 2
Design of experiments using the Box-Behnken method to optimize the Lipo-Let formulation.

Run	Levels of independent variables			Dependent variables		
	DSPC: cholesterol, mol ratio	Sonication time, min	Drug concentration, μg/mL	Average size (nm)	PDI	Entrapment Efficiency (EE)-240 nm (%)
1	0	0	0	190.30	0.227	79.25
2	−1	0	1	253.10	0.289	63.31
3	−1	−1	0	316.40	0.431	65.54
4	1	−1	0	233.10	0.332	71.39
5	−1	0	−1	217.80	0.229	62.22
6	1	0	−1	180.10	0.176	63.80
7	−1	1	0	240.20	0.305	66.45
8	0	0	0	189.00	0.213	81.14
9	0	1	−1	159.70	0.235	77.45
10	0	−1	1	238.80	0.358	83.38
11	0	−1	−1	201.30	0.363	66.21
12	1	1	0	168.30	0.221	68.85
13	0	1	1	212.80	0.273	75.32
14	1	0	1	226.70	0.258	74.21
15	0	0	0	175.50	0.242	80.92

EE (%) = The amount of Lipo-Let-PEG/ the amount of initially added Let × 100

2.5. Drug release study and kinetic model

The dialysis diffusion technique (molecular weight 12 KDa) was used to study the *in vitro* release of drugs from Lipo-Let-PEG. 2 mL of the liposomal suspension was placed in a dialysis bag, sealed, and immersed in 50 mL of PBS (pH 6.8, 37 °C) as the releasing or receiving medium and shaken at 300 rpm on a magnetic stirrer. Samples were removed from the buffer compartment at predetermined intervals and replaced with fresh PBS. The optical density of each batch was evaluated using a UV–Vis spectrophotometer at 240 nm, and the number of drugs released was approximated using a standard curve calculation. The total emission was then plotted against time. The Higuchi, Korsmeyer-Peppas, zero-order, and first-order models were used to study the release kinetics [22].

2.6. Stability of formulation

Lipo-Let PEG nanocarriers were stored at ambient and refrigerated for 2 months to study the nanoliposome's stability. PDI, size, and EE% changes were evaluated at intervals (0, 30, and 60 days).

2.7. Cell lines and culture conditions

Human breast cancer MCF-7 cells and human foreskin fibroblasts (HFF) cells were obtained from IBRC (Iranian Biological Resource Center, Tehran, Iran) and cultured at 37 °C in a humidified atmosphere with 5 % CO2 in RPMI 1640 medium containing 10 % fetal bovine serum (FBS) and 1 % penicillin-streptomycin. The HFF cell line was used as a control in all assays.

2.8. Cell proliferation assay

The MTT assay was used to evaluate cell growth. MCF-7 and HFF cell lines were planted (1×10^4 cells/well) on 96-well culture plates and cultured overnight. For the following 24–48 h, these cells were treated with Lipo, Let, Lipo-Let, and Lipo-Let-PEG (12.5–200 μg/mL). Then, 10 μL of MTT solution in PBS (0.5 mg/mL) was added to each well. After 3–4 h, the supernatant was withdrawn, and 100 μL of dimethyl sulfoxide (Sigma, Germany) was added to each well to dissolve the formazan crystals. The microplates were then gently shaken in the dark for 60 min before the absorbance was measured at 570 nm using a Stat FAX303 plate reader [22].

The percentage of cell viability was calculated using the following formula:

Cell Viability (%) = Optical Density $_{570}$ Treatment/Optical Density $_{570}$ Control × 100%

2.9. Apoptosis analysis

The Annexin V/PI staining kit (Cayman, USA) was used to determine the ratio of apoptosis/necrosis caused by Lipo, Let, Lipo-Let, and Lipo-Let-PEG against MCF-7 cells. MCF-7 cells were seeded at 1×10^5 cells per well in a 6-well plate and treated with the IC_{50}

concentrations of Lipo, Let, Lipo-Let, and Lipo-Let-PEG for 48 h. The cells were washed with 200 μL Binding Buffer and centrifuged at 1500 rpm for 5 min. The cells were then treated with 50 μL Annexin V-FITC and PI reagent. The Cells were incubated for 10 min at room temperature in the dark. The final volume was fixed at 200 μL with a binding buffer. The amount of viable, early apoptotic, late apoptotic, and necrotic cells was measured using the FACS Calibur flow cytometer (Becton Dickinson, San Jose, CA). The results were analyzed using Flow-Jo V10 software (Flowjo, USA) [22].

2.10. Cell cycle assay

MCF-7 cells were grown overnight in 6-well plates at a density of 1×10^6 cells per well. Lipo, Let, Lipo-Let and Lipo-Let PEG IC_{50} concentrations were then applied and incubated for 48 h. Initially, cells were seeded in a complete medium in 6-well plates and incubated overnight. After washing with PBS, the cells were treated with different formulations for 48 h. Finally, the cells were fixed with 70 % ethanol (18 h, 4 °C) and stained with 500 μL PI solution (containing RNase) for 20 min in the dark at room temperature, and cell cycle arrest was assessed in 10,000 cells using a FACS Calibur flow cytometer (Becton Dickinson, San Jose, CA). Cell cycle arrest data were analyzed using FlowJo V10 software (Flowjo, OH, USA) [22].

2.11. Statistical analysis

Statistical data were analyzed via GraphPad Prism 6 software and expressed as mean ± SD. A Student t-test was used to compare two independent groups, and an ANOVA test was used to compare multiple samples. A p-value <0.05 was considered significant.

Table 3
Analysis of variance of the quadratic polynomial model for (a) vesicle size, (b) PDI, and (c) EE% of Lipo-Let.

(a) Vesicle size

Source	Sum of squares	Degree of Freedom	Mean square	F-Value	P-Value	Evaluation
Model	21016.64	9	2335.18	6.30	0.0283	significant
A	6011.56	1	6011.56	16.21	0.0101	significant
B	5439.24	1	5439.24	14.66	0.0123	significant
C	3719.53	1	3719.53	10.03	0.0249	significant
AB	32.49	1	32.49	0.088	0.7792	
AC	31.92	1	31.92	0.086	0.7810	
BC	60.84	1	60.84	0.16	0.7022	
A^2	4632.50	1	4632.50	12.49	0.0167	significant
B^2	1353.46	1	1353.46	3.65	0.1144	
C^2	3.19	1	3.19	8.594E-003	0.9297	

(b) PDI

Source	Sum of squares	Degree of Freedom	Mean square	F-Value	P-Value	Evaluation
Model	0.064	9	7.114E-003	11.11	0.0082	significant
A	8.911E-003	1	8.911E-003	13.91	0.0136	significant
B	0.025	1	0.025	39.51	0.0015	significant
C	3.828E-003	1	3.828E-003	5.98	0.0583	significant
AB	5.625E-005	1	5.625E-005	0.088	0.7789	
AC	1.210E-004	1	1.210E-004	0.19	0.6820	
BC	4.622E-004	1	4.622E-004	0.72	0.4344	
A^2	6.081E-004	1	6.081E-004	0.95	0.3746	
B^2	0.025	1	0.025	38.84	0.0016	significant
C^2	1.733E-005	1	1.733E-005	0.027	0.8758	

(c) EE% of Lipo-Let

Source	Sum of squares	Degree of Freedom	Mean square	F-Value	P-Value	Evaluation
Model	736.69	9	81.85	46.34	0.0003	significant
A	53.72	1	53.72	30.41	0.0027	significant
B	0.30	1	0.30	0.17	0.6972	
C	88.05	1	88.05	49.85	0.0009	significant
AB	2.98	1	2.98	1.68	0.2510	
AC	21.72	1	21.72	12.29	0.0172	significant
BC	93.12	1	93.12	52.72	0.0008	significant
A^2	450.19	1	450.19	254.88	<0.0001	significant
B^2	6.60	1	6.60	3.74	0.1110	
C^2	45.48	1	45.48	25.75	0.0039	significant

3. Results and discussion

3.1. Design study of Lipo-Let

Table 2 shows the effect of the independent variables' levels, including the DSPC to cholesterol ratio, sonication time, and drug concentration, on the study's dependent variables, including PDI, encapsulation percentage, and vesicle size. To select the optimal formulation, 15 runs with different levels of independent variables were performed using the Box-Behnken method. The experimental design using this method determined vesicle size between 159.7 and 316.4 nm, PDI between 0.176 and 0.431, and percentage of EE between 62.22 and 83.38 %.

Polynomial linear regression was also performed to statistically calculate the effect of the independent variables on the dependent variables. Analysis of variance of the quadratic polynomial model for particle size indicated that all three independent variables factors contributed to size changes (Table 3a). The analysis of variance of the quadratic polynomial model for PDI indicated that all three independent variables contributed to PDI changes (Table 3b). Also, this analysis for the percentage of encapsulation efficiency showed that the ratio of DSPC to cholesterol and drug concentration had a potential effect on EE% changes, but sonication time did not significantly affect EE% of nanoliposomes (Table 2).

The experimental design was also performed using Design Expert software, and the effects of different levels of independent variables on changes in size, PDI, and EE% were schematically shown. According to Fig. 1a-c, it can be said that at high levels of the DSPC to cholesterol ratio, the nanoliposome size decreases with increasing sonication time. Although at high levels of the ratio of DSPC to cholesterol, the size of nanoparticles increased with increasing drug concentration. In addition, an increase in the sonication time and drug concentration led to an observed increase in the nanoliposome's vesicle size.

Fig. 1d-f shows that at high DSPC to cholesterol ratios, the PDI of the nanoliposomes decreases dramatically with the increase of the sonication time. Although at higher DSPC to cholesterol ratio levels, the PDI slightly increases with increasing drug concentration. A significant increase in PDI was also observed by increasing the sonication time and drug concentration.

As shown in Fig. 1g-i, at low levels of the ratio of DSPC to cholesterol, the EE% of nanoliposomes increased with enhancement of sonication time, but at higher levels of independent variable A, the EE% of nano-vehicle enhanced with elevation of sonication time. Also, at intermediate levels of the ratio of DSPC to cholesterol, the EE% increased with increasing drug concentration. In addition, increased EE% of the Lipo-Let formulation at all levels of sonication time was reported with increasing drug concentration.

The results of the regression analysis for the size and PDI of the responses to fit the quadratic model are shown in Tables 3a and 3b, respectively, which indicate that the variables of the ratio of DSPC to cholesterol and the sonication time have a negative effect (decreasing), and the drug concentration has a positive effect (increasing) on the size and PDI of Lipo-Let formulation.

Table 3c also shows the fitted model for the EE% of the responses, which shows the positive effect (increasing) of all three independent variables on the EE%.

Cholesterol is an organic sterol molecule that comprises a large steroid ring with a malleable carbohydrate and a hydroxyl group and can form hydrogen bonds with phospholipids. The eukaryotic cell membrane contains the 27-carbon molecule cholesterol, which makes up approximately 30–50 mol% of all lipid molecules in the membrane. Cholesterol controls membranes' permeability,

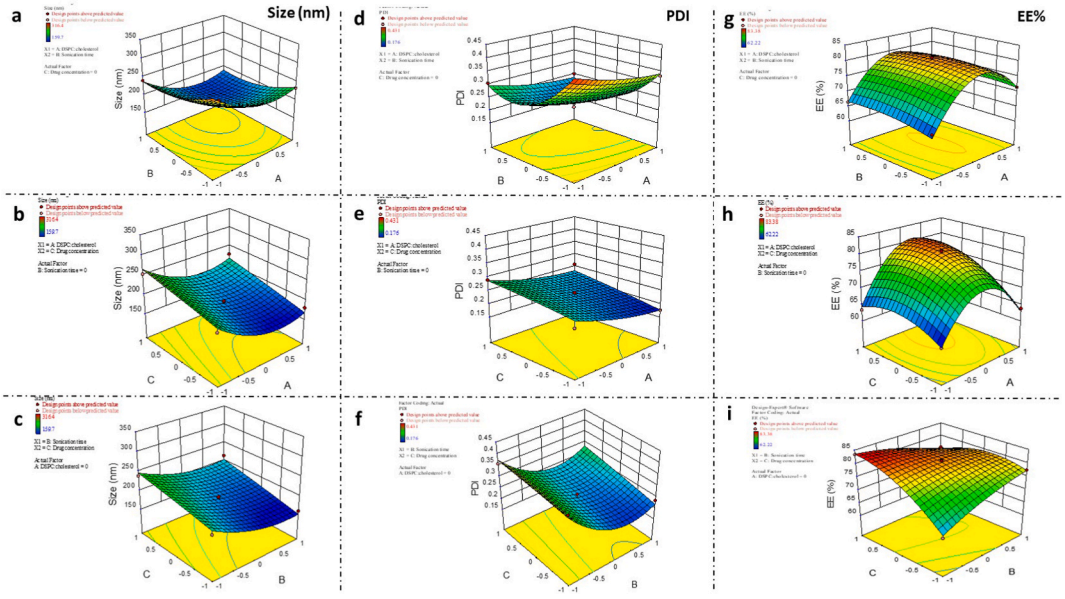

Fig. 1. Designing the experiment based on the effects of independent variables on the (a-b-c) vesicle size, (d-e-f) PDI, and (g-h-i) %EE of Lipo-Let using Design Expert software.

elasticity, and rigidity, among other crucial functions. The most common sterol utilized in liposome formulation is cholesterol, which can increase the strength of the liposomal membrane while avoiding liposome agglomeration [23,24].

The cholesterol content of liposomes can vary and customize the phospholipid packaging, membrane fluidity, and surface charge, which impacts particle size, encapsulation efficiency, and ultimate morphology. Cholesterol has fascinating effects on the zeta potential, remarkably increasing the zeta potential of cationic liposomes. The hypothesized strategy for cholesterol-induced charge enhancement of cationic liposomes depends on modifying membrane shape and molecular filling state. The transition from the crystalline state to the liquid-ordered (LO) phase can be brought on by cholesterol. The average size of liposomes can be raised by boosting the quantity of cholesterol in their membrane. Hydrophobic interactions and hydrogen bonding between the cholesterol structure and the phospholipid hydrophobic acyl chain are made possible by the hydrophobic nature of both molecules. The relatively rigid ring structure of cholesterol stabilizes the extended straight-chain arrangement of saturated fatty acids through van der Waals interactions [25,26].

It has been reported that EE% may decrease with higher cholesterol and drug concentrations. The incorporation of hydrophobic compounds may be favored by the fact that cholesterol makes the core of the membrane bilayer more hydrophobic. Conversely, because both cholesterol and the drug prefer to localize in the hydrophobic part of the membrane, and because there is only a tiny amount of space available for both, cholesterol and hydrophobic drug molecules may compete for the available space within the acyl chains of the phospholipids, leading to decreased packaging as the cholesterol content increases. Therefore, the higher DSPC/cholesterol ratio and the upper drug concentration may result in more excellent drug encapsulation [27].

DSPC has a high phase-transition temperature (Tm = 55 °C) and is compatible with cholesterol. It contains two fully saturated fatty acids, both stearic acid. Lipid bilayers often go through one of two thermodynamic phases: gel or liquid-crystal. Because the hydrocarbon chains are fully stretched and tightly packed, the lipid membrane is in the gel phase at Tm, which is relatively compact and rigid due to the reduced energy of random motion of the lipid molecules. Liposomes composed of phospholipids, such as DSPC, are more stable than those composed of unsaturated fatty acids, such as egg phosphatidylcholine (PC), or fatty acids with shorter or irregular carbon chains, such as hydrogenated soybean PC (HSPC) [28]. Cholesterol disintegrates in the phospholipid bilayer rather than forming a separate bilayer.

It has been suggested that higher cholesterol levels prevent the phospholipid bilayer from packing tightly because they increase membrane fluidity, which causes an increase in the dispersion of the aqueous phase within the liposomal vesicles. This explains why the mean liposome diameter decreased as the DSPC/cholesterol ratio increased [29].

3.2. Study of the optimal structure of Lipo-Let

After conducting a prediction study on the effect of independent variables on the size, PDI, and %EE of Lipo-Let formulation, appropriate and desirable levels of independent variables were predicted. According to Table 4, the ratio of DSPC to cholesterol, sonication time, and drug concentration for the most optimal formulation was calculated as 1.8 M ratio, 5.56 min, and 514.75 μg/mL. The desirability of the optimal structure was reported to be 0.767.

Table 5 shows the average size, PDI, %EE, and zeta potential charge for Lipo, Lepo-Let, and Lipo-Let-PEG in the responses obtained by the Box-Behncken and experimental methods. According to this table, the vesicle size of Lipo-Let-PEG in the experimental method was equal to 170.05 ± 4.15 nm, its PDI was equal to 0.154 ± 0.010, %EE was equal to 1.36 ± 87.21 and with a negative zeta charge, which compared to the optimal formulation predicted by Box-Behncken method had a smaller size and PDI and higher %EE.

4. Physicochemical identification tests of Lipo-Let-PEG

4.1. Morphological tests

FE-SEM and DLS techniques were used to investigate the morphology and size of the optimized Lipo-Let-PEG formulation (Fig. 2a and b). FE-SEM images of the optimized Lipo-Let PEG formulation are shown in Fig. 2a, which shows that the nanoliposomes have a uniform spherical morphology with a smooth surface. Fig. 2b shows the dynamic diameter graphs of Lipo, Lipo-Let, and Lipo-LET-PEG formulations, estimated to be 133.60, 197.80, and 170.05 nm, respectively. The reduction in vesicle size of liposomes after PEGylation may be due to the increase in repulsive forces on the liposome surface [30].

4.2. Cumulative drug release study and kinetic model analysis

Drug release from Lipo and Lipo-PEG was investigated at pH 5.4 and 7.4, as shown in Fig. 2c. According to this figure, it was shown that in the first 12 h, explosive drug release was witnessed from both structures at both pH levels. Subsequently, the drug release slope decreased, and the maximum drug release was observed at 72 h. This means that the release of the drug after 72 h from the Lipo

Table 4
Desirability criteria and predicted values for the independent variables of the experiment.

Number	DSPC: cholesterol, moL ratio	Sonication time, min	Drug concentration, μg/mL	Desirability
1	1.8	5.56	514.75	0.767

Table 5
Optimum responses obtained by Box-Behnken method and experimental data for the same responses in optimal conditions.

Parameter	Predicted by Box-Behnken	Lip-Let	Lip-Let -PEG	Liposome (Lip)
Average size (nm)	182.02	197.80 ± 6.20	170.05 ± 4.15	133.60 ± 4.50
PDI	0.202	0.184 ± 0.016	0.154 ± 0.010	0.076 ± 0.011
Entrapment Efficiency (EE) (%)	75.418	80.38 ± 1.95	87.21 ± 1.36	–
Zeta potential (mV)	–	−24.30 ± 1.22	−19.80 ± 1.64	−31.50 ± 1.97

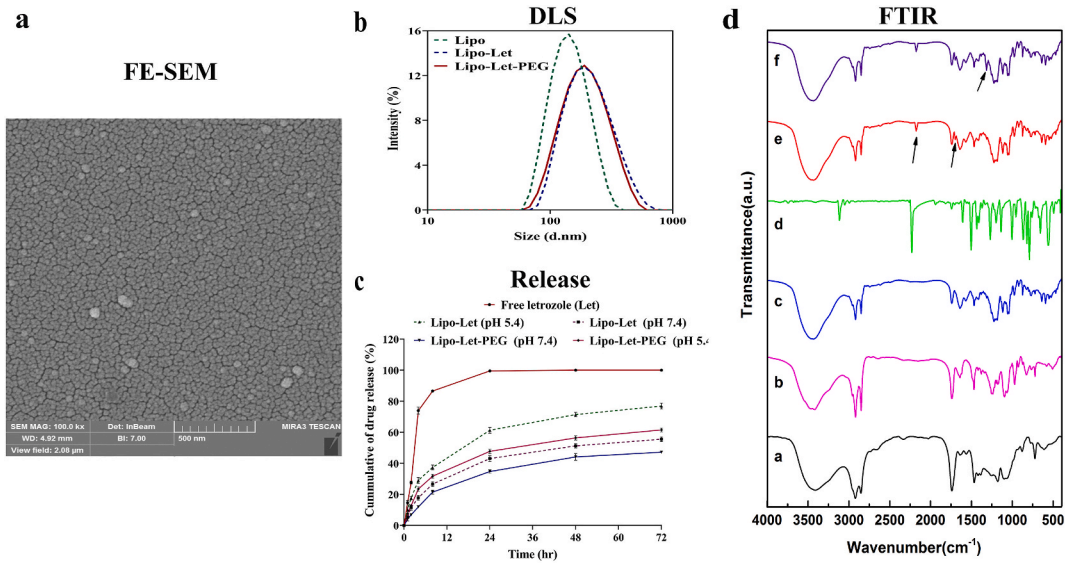

Fig. 2. (a) FE-SEM graphs of Lipo-Let-PEG. (b) Dynamic diameter graphs of Lipo, Lipo-Let, and Lipo-Let-PEG formulations. (c) Let release from liposomal structure and PEGylated liposome at two pH values of 5.4 and 7.4. (d) FTIR image of (a) cholesterol, (b) distearoylphosphatidylcholine (DSPC), (c) Lipo, (d) Let, (c) Lipo-Let, and (f) Lipo-Let-PEG formulations.

structure at pH 5.4 is approximately equal to 80 %, and from the Lipo structure at pH 7.4 is almost equal to 55 %. The cumulative release from the Lipo-Let-PEG at pH 5.4 and 7.4 was also approximately 60 % and 50 %, respectively. PEG prevents the drug from being released from nanoparticles by covering their surface. For the use of nanoparticles, premature drug release is a challenge that might be overcome by PEGylation [31]. In addition, Papp et al. showed that PEGylated liposomes synthesized by the reverse phase method resulted in less drug release after 48 h than non-PEGylated liposomes synthesized by the reverse phase method [32].

Table 6 also shows the results of the analysis of kinetic models for Let release from the prepared structures. The study of drug kinetic models revealed that the release of Let from both Lipo and Lipo-PEG structures followed Higuchi and Korsmeyer-Peppas kinetics. However, the free drug release followed the first-order model. In the Korsmeyer-Peppas model, the rate of drug release is controlled by the rate of diffusion and swelling. However, in the Higuchi kinetic model, the cumulative drug release amount is proportional to the square root of time [33,34].

4.3. FTIR analysis

Chemical interactions to detect drug loading in the liposome structure and PEGylation of this structure were investigated using the

Table 6
Proposed kinetic models for the release of Let from liposomal structure and PEGylated liposome at pH 5.4 and 7.4.

Release Model	Equation	R^2				
		Nio-Let (pH = 7.4–37 °C)	Nio-Let (pH = 5.4–37 °C)	Nio-Let-PEG (pH = 7.4–37 °C)	Nio-Let-PEG (pH = 5.4–37 °C)	Free letrozole (Let) (pH = 7.4–37 °C)
Zero-order	$C_t = C_0 + K_0 t$	$R^2 = 0.8364$	$R^2 = 0.8309$	$R^2 = 0.8556$	$R^2 = 0.8251$	$R^2 = 0.4604$
First-order	$LogC = LogC0 + K_t/2.303$	$R^2 = 0.8929$	$R^2 = 0.6256$	$R^2 = 0.8974$	$R^2 = 0.8968$	$R^2 = 0.9153$
Higuchi	$Q = K_H \sqrt{t}$	$R^2 = 0.9519$	$R^2 = 0.9481$	$R^2 = 0.9621$	$R^2 = 0.9436$	$R^2 = 0.6292$
Korsmeyer-Peppas	$M_t/M_\infty = K_t^n$	$R^2 = 0.9445$ $n = 0.5227$	$R^2 = 0.9605$ $n = 0.4567$	$R^2 = 0.9661$ $n = 0.5825$	$R^2 = 0.9475$ $n = 0.4734$	$R^2 = 0.7441$ $n = 0.4085$

FTIR technique. Fig. 2d (a) shows the FTIR of cholesterol, where the peaks related to the bending and deformation of CH2 bonds appeared in the regions of 1036–1389 cm^{-1}, respectively, and the peaks related to the stretching C–C bond of the aromatic ring appeared sharply in the region of 1517 cm^{-1}. In addition, there are various peaks obtained, including the peaks related to C=C double bond in the region of 1674 cm^{-1} and the peak related to C=O stretching bond in the region of 1728 cm^{-1}, as well as the peaks in the regions of 2863–3124 cm-1 which are related to C–H stretching bond. The broad peak at 3452 cm^{-1} is related to the OH stretching bond.

Fig. 2d (b) shows the FTIR of DSPC, the peaks accompanied by the P–O bond in the region of 826–722 $cm^{-1,}$ and the bands related to the stretching bond P=O in the region of 1243 cm^{-1} and the C–N bond in the region of 1000–1350 cm^{-1} appeared. The band related to the CH3-methyl bond appeared at 1374 $cm^{-1,}$ and the band related to the CH2-chain bond appeared at 1465 cm^{-1}.

Fig. 2d (c) indicates the FTIR of the liposome, which represented the leading characteristic bands of the liposome, especially those due to the symmetric and antisymmetric P=O vibrational stretching bonds in the 1045 and 1214 cm^{-1} regions. CH2 bending vibration in 1749 cm^{-1} region and carbonyl C=O stretching vibration in 1749 cm^{-1} and OH stretching and bending vibration appeared in 3478 and 1645 cm^{-1} regions, respectively.

Fig. 2d (d) shows the FTIR of Let, where the peaks related to N–H out-of-plane bending, C–N stretching, and N–H bending are visible in the regions of 800, 1350–1000, and 1550-1640 cm^{-1}, respectively. 1550-1640 cm^{-1}, and the weak stretching absorption peaks correlated to C=C of the aromatic ring of Let were visible in the 1450-1600 cm^{-1} region.

Fig. 2d (e) shows the FTIR of Let loaded in the liposome, which indicates that by adding Let to the liposome structure, the bands related to Let bonds were observed. The band associated with Let in the region of 2180 cm^{-1} (C ≡ N stretching bond) and 1698 cm^{-1} (C=N bond) can confirm the successful loading of Let on the liposome structure.

Fig. 2d (f) indicates the FTIR of Lipo-Let-PEG formulation, which exhibits that after the PEGylation of the Lipo-Let, the bands accompanied by Let are still observed with some shift to shorter wavelengths. The PEGylation of the structure revealed the sharp band associated with the C–H bond of PEG in the region of 1315 cm^{-1}, which may be a reason for the PEGylation of the structure.

4.4. Storage stability analysis

The stability of nanoparticles is essential for their development, storage, and efficacy in drug delivery into the bloodstream [35]. The stability of the prepared Lipo-Let and Lipo-LET-PEG formulation was compared at two temperatures of 25 °C and 4 °C for two months (Fig. 3a-f). According to Fig. 3a and c, it was shown that there was a significant increase in size and PDI of Lipo-Let after two months of storage at 25 °C compared to 4 °C ($P < 0.001$) and this increase was also evident after one month, but changes were made less than 2 months of storage ($P < 0.01$ for size and $P < 0.05$ for PDI). However, a significant decrease in %EE was observed only after 2 months of storage at room temperature compared to refrigerator temperature ($P<0.001$) (Fig. 3e). Fig. 3b, d, and 3f also showed that the results of the change in size, PDI, and %EE of Lipo-Let-PEG stored at 25 °C compared to 4 °C were similar to those of Lipo-Let ($P<0.001$ and $P<0.01$). These results indicated that the PEGylated structure was more effective in protecting their size, PDI, and EE% from changes than their non-PEGylated counterparts.

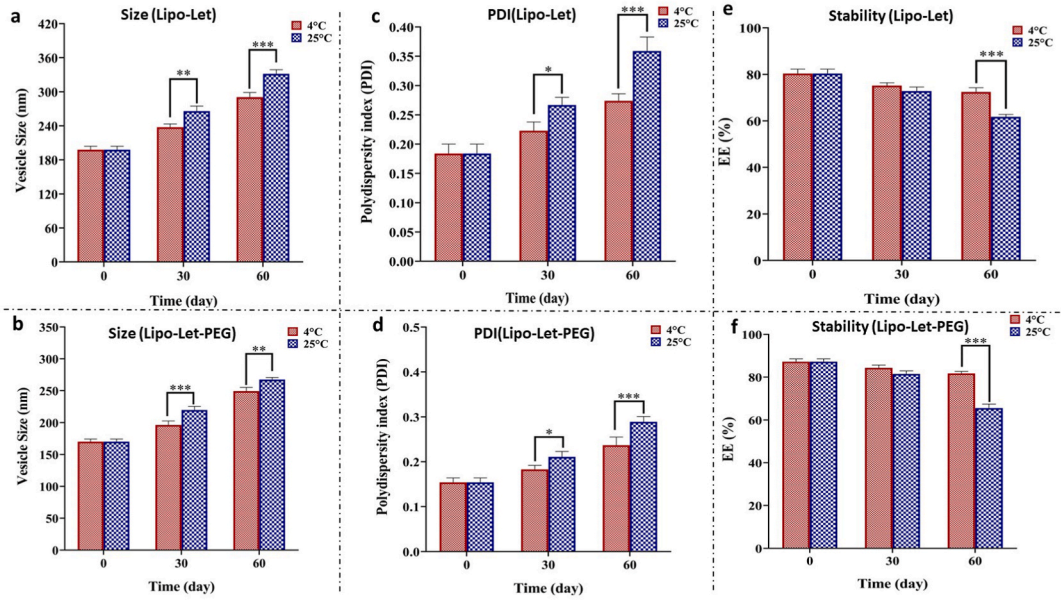

Fig. 3. The alteration of vesicle size of (a) Lipo-Let and (b) Lipo-Let-PEG, PDI of (c) Lipo-Let and (d) Lipo-Let-PEG and %EE of (e) Lipo-Let and (f) Lipo-Let-PEG at two temperatures of 25 °C and 4 °C for two months. (*: $P < 0.05$, **: $P < 0.01$ and ***$P < 0.001$).

5. Cell cytotoxicity assay

5.1. MCF-7 and HFF cells viability

The therapeutic properties of drugs can be improved by using liposomes as drug carriers [20]. Liposomes can increase the amount of drug inside tumor cells by prolonging the drug's circulation time. They can transport drugs to the intended regions *in vivo*, thus preventing adverse drug effects on healthy cells [20]. In the current study, Fig. 4a and b shows the anticancer effect of different concentrations (12.5–200 μg/mL) of Lipo, Let, Lipo-Let, and Lipo-Let-PEG against MCF-7 cancer cell line during 24 and 48 h, respectively. It can be observed that all formulations at all time intervals and all concentrations were able to cause a significant decrease in the survival of cancer cells ($P<0.001$). However, 48-h treatment of all formulations at all concentrations except empty Liposome could cause a dramatic decrease in cancer cell viability compared to 24-h treatment ($P<0.001$). The 48-h treatment with a 200 μg/mL concentration of Lipo-Let-PEG induced the highest reduction in cancer cell viability ($P<0.001$). From the results of this study, it can be concluded that the Lipo-Let-PEG formulation showed the highest anticancer effect against MCF-7 cells, and its anticancer effect was more significant during the 48-h treatment. Fig. 4d shows the IC_{50} values of Lipo, Let, Lipo-Let, and Lipo-Let-PEG against the MCF-7 cancer cell line at 24 and 48 h. The IC_{50} values of Lipo-Let-PEG were significantly lower than those of the other groups at both time points ($P < 0.001$).

The IC_{50} values of Lipo, Let, Lipo-Let, and Lipo-Let-PEG against the MCF-7 cancer cell line were 3688, 395, 144, and 50.16 μg/mL for 24 h and 2774, 119.5, 57.58 and 18.60 μg/mL for 48 h treatment, respectively. Fig. 4c shows the anticancer effect of different concentrations (12.5–200 μg/mL) of Lipo, Let, Lipo-Let, and Lipo-Let-PEG formulations against regular HFF cell lines within 24 h. As shown in the graph, all the formulations showed a high level of biocompatibility with normal HFF cells. The encapsulation of Let in the liposomal structure indicates lower toxicity against HFF cells than that of the pure drug. Moreover, PEGylation reduced the general cytotoxicity associated with liposomes (impact on normal cells).

Overall, the results showed that Lipo-Let-PEG produced more drug cytotoxicity than Lipo-Let. This may be because Lipo-Let-PEG has a higher EE% than Lipo-Let, is smaller in size, and releases the drug differently. These results were consistent with those of Najlah et al., who found that disulfiram-loaded PEGylated liposomes induced more significant cytotoxicity against human colon cancer H630 WT and 5FU-resistant human colon cancer H630 R10 cells compared to disulfiram loaded non-PEGylated liposomes [36]. The results of different studies in rats with breast cancer showed that the cytotoxic effects of cisplatin encapsulated in PEGylated liposomes were increased by a factor of 2.4 and 1.9 after 24 and 48 h, respectively [20]. According to the results of the study by Ghaferi et al.,

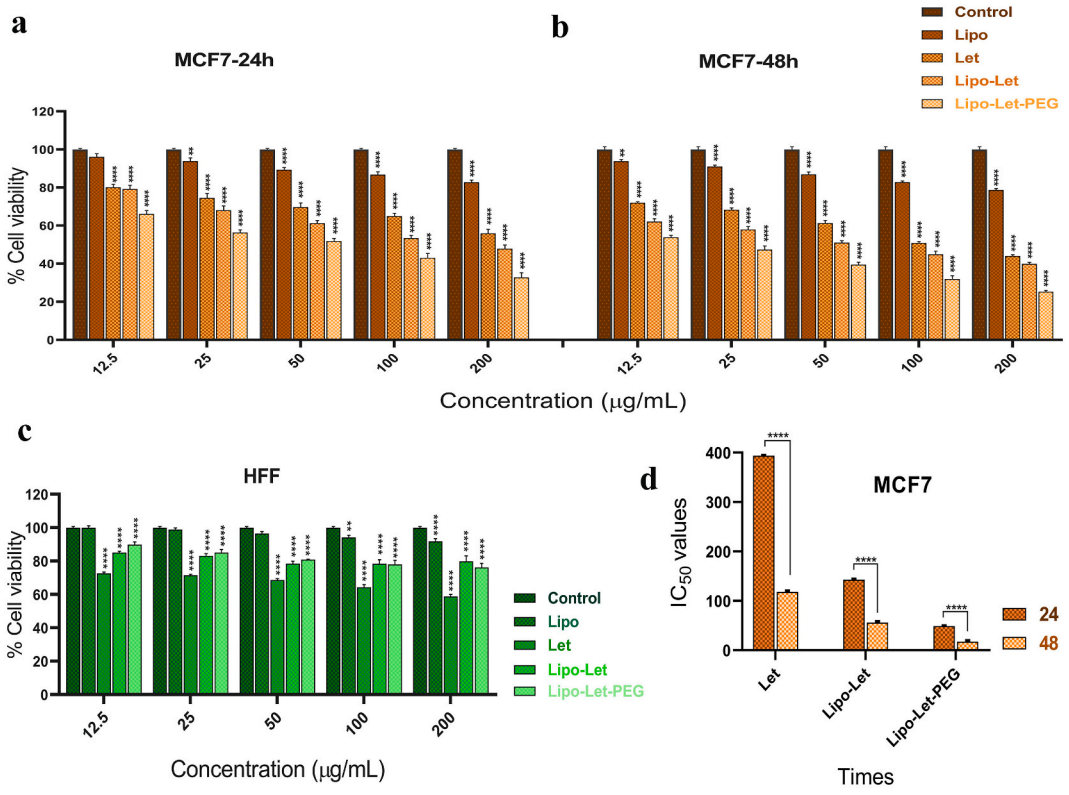

Fig. 4. The anticancer effect of different concentrations (12.5–200 μM) of Lipo, Let, Lipo-Let, and Lipo-Let-PEG formulations against MCF7 cancer cell line during (a) 24 and (b) 48 h and (c) against HFF normal cells for 24 h. (d) The comparison of IC_{50} concentration of Lipo, Let, Lipo-Let, and Lipo-Let-PEG formulations against MCF-7 cancer cell line during 24 and 48 h (*: $P < 0.05$, **: $P < 0.01$ and ***$P < 0.001$).

doxorubicin and carboplatin were encapsulated in uncoated liposome and PEGylated liposome, which increased the cytotoxic effects of the drugs against glioblastoma cancer cells. PEGylated liposomes prompted drug cytotoxicity compared to liposomes [37].

Evidence suggests that the enhanced cellular uptake of PEGylated nanoparticles in cancer cells can be attributed to several factors. When nanocarriers are pegylated, they acquire specific properties that facilitate their interaction with cancer cells, leading to improved uptake. PEGylation of liposomes could enhance cellular uptake in cancer cells by increasing circulation time steric stabilization, enabling targeted delivery, leveraging synergistic effects, improving stability and drug release, and reducing aggregation. These factors collectively contribute to a more effective interaction between PEGylated vesicles and cancer cells, ultimately enhancing cellular uptake for improved therapeutic outcomes. Steffes et al. showed that PEGylation of liposomes dramatically improves the delivery and cytotoxicity of paclitaxel (PTX) to human melanoma (M21) and prostate cancer (PC3) cells. The PEG-coated nanoparticles were shown to be sterically stable, maintaining the nanoparticles' small size and preventing the nanoparticles' adhesion to the cell medium. This appears to be a critical factor in promoting the uptake and delivery of PTX through various size-mediated endocytosis pathways [38,39].

Other researchers have reported that the superior *in vitro* cytotoxic activity of PEGylated niosomal formulations are also present. For example, PEGylated noisome showed higher cytotoxicity against the HepG2 cells [40]. In addition, another study demonstrated a more potent cytotoxic activity against lung cancer TC-1 cells than the free drug [41].

The specific impact of PEGylation on cellular uptake can vary depending on factors such as the length of the PEG chain. For instance, research comparing liposomes with different PEG chain lengths (e.g., PEG750 and PEG2000) has demonstrated that longer PEG chains may reduce pH responsiveness but not necessarily decrease cellular uptake [42].

Limitations of this study include lacking cellular uptake of letrozole-encapsulated PEGylated nanoliposomes and *in vivo* experimental studies.

In vivo and clinical studies will provide in-depth insight into the precise anticancer effects of letrozole-encapsulated PEGylated nanoliposomes. Therefore, the most appropriate way to study the efficacy of drug delivery systems is through a combination of *in vitro*, *in vivo*, and human studies. For this reason, screening in cell culture is acceptable as a first stage, followed by evaluating the best formulation in cell culture for animal studies. The optimized formulation could then be tested in clinical trials.

5.2. Lipo-Let-PEG induced apoptosis in MCF-7 cancer cells

Finding novel anticancer treatments that target the apoptotic pathway is an appealing strategy since it is cancer-type-unspecific. Therefore, the cells treated with IC_{50} concentrations of Lipo, Lipo-Let, and Lipo-Let-PEG were assessed using Annexin V-FITC binding analysis and PI staining to measure MCF-7 death rates resulting from necrosis and apoptosis. According to Fig. 5a-e, only 1.604 % of

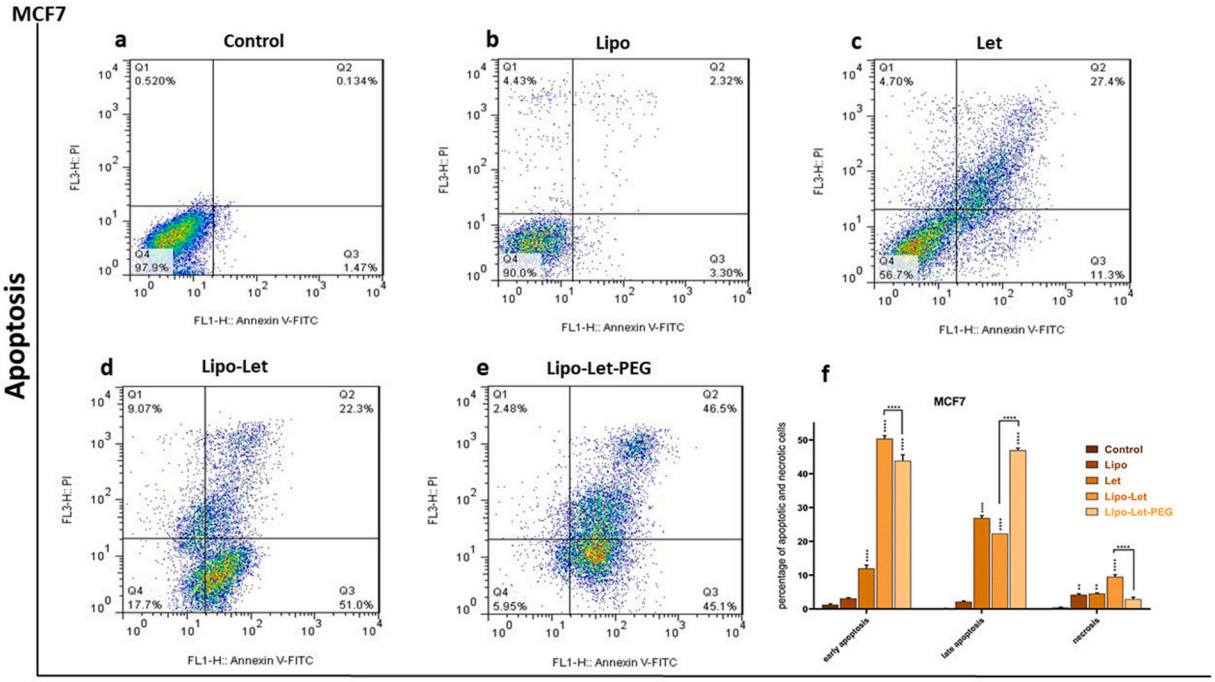

Fig. 5. The effects of IC_{50} concentration of (b) Lipo, (c) Let, (d) Lipo-Let, and (e) Lipo-Let-PEG on apoptosis of MCF-7 cells compared to the (a) control group. MCF-7 cells were double-stained with Annexin V/propidium iodide and assessed by flow cytometry. Untreated cells were indicated as control. Diagrams quarter 1 (Q1) to Q4 indicate necrotic, late apoptotic, early apoptotic, and live cells, respectively. (f) The comparative analysis of apoptosis and necrosis occurrence in cells treated with Lipo, Let, Lipo-Let, and Lipo-Let-PEG after 48 h (*: $P < 0.05$, **: $P < 0.01$ and ***$P < 0.001$).

the cells in the control group were apoptotic. Treatment with Lipo-Let and Lipo-Let-PEG significantly increased the number of Annexin V-FITC/PI-positive cells. The percentage of MCF-7 in the late apoptotic stage after application of Lipo, Let, Lipo-Let, and Lipo-Let-PEG at concentrations of IC_{50} was approximately 2.60 %, 19.35 %, 22.3 %, and 58.10 %, respectively, and in the early apoptotic stage was 3.50 %, 12 %, 50.35 %, and 43.85 %, respectively. Flow cytometry analysis also revealed that the percentage of necrotic MCF-7 cells after administration of Lipo, Lipo-Let-PEG at IC_{50} concentration was 2.90 %. The statistical results obtained from the apoptosis study using flow cytometry showed that Lipo-Let-PEG caused the most significant decrease in cancer cell viability and also the most remarkable occurrence of apoptosis in cancer cells compared to other treated groups ($P < 0.001$) (Fig. 5f).

In addition, the lowest level of necrosis was induced in cancer cells after treatment with Lipo-Let-PEG, demonstrating the high anticancer activity of this formulation. Compared to Lipo-Let and the drug alone, the results showed that Lipo-Let-PEG could significantly increase the induction of apoptosis in cancer cells. This was consistent with the improvement in cytotoxicity, suggesting a relationship between intracellular drug levels and tumor inhibition efficacy. According to the work of Wen et al., non-targeted shikonin-loaded liposomes (SSLs-SHK) and RGD-SSLs-SHK could also clearly induce apoptosis by decreasing BCL2 expression and increasing BAX expression [43]. Consistent with the flow cytometry results, Yang et al. found that PEGylated liposomal oxaliplatin-induced a more excellent apoptotic response in colon cancer cells than empty PEGylated liposomes or free oxaliplatin [44].

5.3. Lipo-Let-PEG-induced cell cycle arrest

Cell cycle parameters were also tested in Lipo, Let, Lipo-Let, and Lipo-Let-PEG-treated MCF-7 cells after 48 h of treatment. Hoechst indicators were used to determine the DNA content of the cells, and after numerous cells were gated out to create DNA content histograms, areas corresponding to G1, S, and G2 DNA content levels were identified [45]. Cell cycle analysis showed that most cells were arrested in the sub-G1 phase. According to Fig. 6a-e, the sub-G1 MCF-7 cell population in control cells and cells treated with Lipo, Let, Lipo-Let, and Lipo-Let-PEG was 0.82 %, 15.30 %, 18.00 %, 25.11 %, and 67.60 %, respectively. It also showed that IC_{50} treatment of Lipo-Let-PEG caused a significant reduction in cell arrest in the G1 and S phases of the cell cycle compared to other groups ($P < 0.001$). All treatments also cause a remarkable decrease in G2 phase cell frequencies compared to control ($P < 0.001$) (Fig. 6f).

According to Sriraman et al., liposomal-loaded cobimetinib mainly caused cell cycle arrest in the G1 phase and prevented colorectal cancer cells from progressing into the S-phase. The impact on the regulation of cell cycles is accompanied by the onset of apoptosis [46]. The accurate regulation of G1 phase occurrences by the G1 phase cyclins may be the mechanism of action for these results. Cyclin A, a regulatory protein required for a cell to transition from the G1 to S phase, is a rate-limiting factor [47]. By preventing uncontrolled entry into the S phase in the presence of DNA-damaging chemicals, Cyclin D1 controls a G1/S checkpoint. Cyclin D1 accelerates passage through G1 but prevents entry into the S phase. According to Tung et al.'s experiment, treatment of colorectal cancer cells with PEGylated-liposomal oxaliplatin led to impeded DNA synthesis and a considerably shorter S-phase, while expression of Cyclin A was lowered and Cyclin D1 was elevated [48,49]. Therefore, it was reported that the number of cells in the G1 and S-phases decreased and in the sub-G1 phase increased after treatment with Lipo-Let-PEG compared to empty drug and non-PEGylated nanocarrier.

6. Conclusion

In conclusion, as the complicated scenario of breast cancer, the results reported in the current investigation support our hypothesis of an alternative drug delivery strategy that specifically targets breast cancer cells and induces apoptosis in the MCF-7 cell line. The future perspective of this article is the application of letrozole-encapsulated PEGylated nanoliposomes (Lipo-Let-PEG) as a delivery system to breast cancer cells, potentially inhibiting cancer cell proliferation or inducing cancer cell apoptosis. In addition, Lipo-Let-PEG can be used as an anticancer agent by arresting cell cycle progression, which can be applied in future studies to prevent tumor development.

This project lacks cellular uptake data and *in vivo* studies. Understanding how efficiently the cells internalize the nanoliposomes would provide insights into the mechanism of letrozole delivery and its potential effectiveness. Assessing the anticancer activity of the formulation in an animal model is a critical step. *In vivo* experiments would provide valuable information on the biodistribution, pharmacokinetics, and therapeutic efficacy of the PEGylated nanoliposomes within a whole organism.

Data availability

The manuscript contains the data sets used in the current study.

Ethics approval and consent to participate

Not applicable.

Consent for publication

All authors consent to the publication of this study.

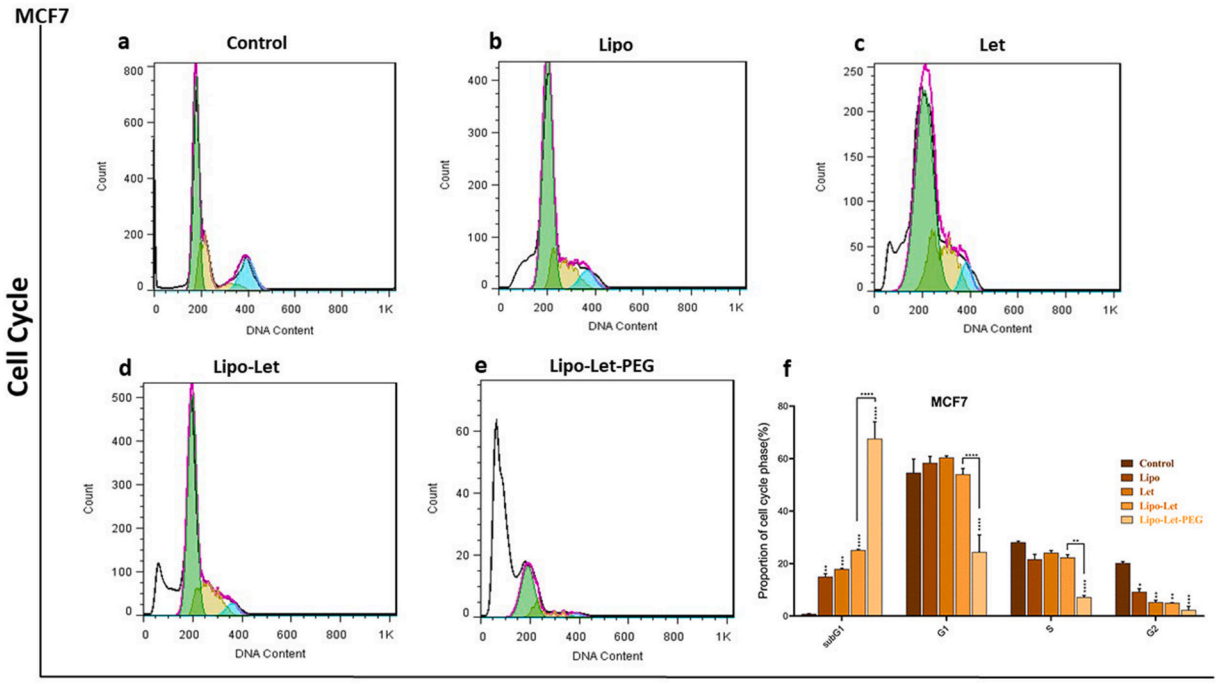

Fig. 6. The effects of IC_{50} concentration of (b) Lipo, (c) Let, (d) Lipo-Let, and (e) Lipo-Let-PEG on cell cycle arrest of MCF-7 cells compared to the (a) control group. (f) The comparative analysis of cell cycle arrest in sub-G1, G1, S, and G2 phases in MCF-7 cells treated with Lipo, Let, Lipo-Let, and Lipo-Let-PEG after 48 h (*: $P < 0.05$, **: $P < 0.01$ and ***$P < 0.001$).

Availability of data and materials

The datasets used and/or analyzed during the current study are available from the corresponding author on reasonable request.

Funding

There is no funding.

CRediT authorship contribution statement

Soraya Shahbazi: Writing – original draft, Methodology, Formal analysis, Data curation. **Farzaneh Tafvizi:** Writing – review & editing, Supervision, Project administration, Methodology, Data curation. **Vahid Naseh:** Methodology.

Declaration of competing interest

The authors declare that they have no known competing financial interests or personal relationships that could have appeared to influence the work reported in this paper.

References

[1] Z. Li, T. Guo, S. Zhao, M. Lin, The therapeutic effects of MUC1-C shRNA@ Fe3O4 magnetic nanoparticles in alternating magnetic Fields on Triple-negative breast cancer, Int. J. Nanomed. (2023) 5651–5670.
[2] J. Nel, K. Elkhoury, É. Velot, A. Bianchi, S. Acherar, G. Francius, et al., Functionalized liposomes for targeted breast cancer drug delivery, Bioact. Mater. 24 (2023) 401–437.
[3] N. Azamjah, Y. Soltan-Zadeh, F. Zayeri, Global trend of breast cancer mortality rate: a 25-year study, Asian Pac. J. Cancer Prev. APJCP: Asian Pac. J. Cancer Prev. APJCP 20 (7) (2019) 2015.
[4] D-x He, X. Ma, Clinical utility of letrozole in the treatment of breast cancer: a Chinese perspective, OncoTargets Ther. (2016) 1077–1084.
[5] A. Yassemi, S. Kashanian, H. Zhaleh, Folic acid receptor-targeted solid lipid nanoparticles to enhance cytotoxicity of letrozole through induction of caspase-3 dependent-apoptosis for breast cancer treatment, Pharmaceut. Dev. Technol. 25 (4) (2020) 397–407.
[6] B. Alemrayat, A. Elhissi, H.M. Younes, Preparation and characterization of letrozole-loaded poly (d, l-lactide) nanoparticles for drug delivery in breast cancer therapy, Pharmaceut. Dev. Technol. 24 (2) (2019) 235–242.
[7] M. Bourbour, N. Khayam, H. Noorbazargan, M.T. Yaraki, Z.A. Lalami, I. Akbarzadeh, et al., Evaluation of anti-cancer and anti-metastatic effects of folate-PEGylated niosomes for co-delivery of letrozole and ascorbic acid on breast cancer cells, Molecular Systems Design & Engineering 7 (9) (2022) 1102–1118.
[8] M.J. Mitchell, M.M. Billingsley, R.M. Haley, M.E. Wechsler, N.A. Peppas, R. Langer, Engineering precision nanoparticles for drug delivery, Nat. Rev. Drug Discov. 20 (2) (2021) 101–124.

[9] E. Beltrán-Gracia, A. López-Camacho, I. Higuera-Ciapara, J.B. Velázquez-Fernández, A.A. Vallejo-Cardona, Nanomedicine review: clinical developments in liposomal applications, Cancer Nanotechnology 10 (1) (2019) 1–40.
[10] Montoto S. Scioli, G. Muraca, M.E. Ruiz, Solid lipid nanoparticles for drug delivery: pharmacological and biopharmaceutical aspects, Front. Mol. Biosci. 7 (2020) 319.
[11] Y. Fan, M. Marioli, K. Zhang, Analytical characterization of liposomes and other lipid nanoparticles for drug delivery, J. Pharmaceut. Biomed. Anal. 192 (2021) 113642.
[12] D.D. Lasic, Novel applications of liposomes, Trends Biotechnol. 16 (7) (1998) 307–321.
[13] M. Gulati, M. Grover, S. Singh, M. Singh, Lipophilic drug derivatives in liposomes, Int. J. Pharm. 165 (2) (1998) 129–168.
[14] P. Ghasemiyeh, S. Mohammadi-Samani, Solid lipid nanoparticles and nanostructured lipid carriers as novel drug delivery systems: applications, advantages and disadvantages, Research in pharmaceutical sciences 13 (4) (2018) 288.
[15] M.K. Riaz, M.A. Riaz, X. Zhang, C. Lin, K.H. Wong, X. Chen, et al., Surface functionalization and targeting strategies of liposomes in solid tumor therapy: a review, Int. J. Mol. Sci. 19 (1) (2018) 195.
[16] P. Liu, G. Chen, J. Zhang, A review of liposomes as a drug delivery system: current status of approved products, regulatory environments, and future perspectives, Molecules 27 (4) (2022) 1372.
[17] L. Sercombe, T. Veerati, F. Moheimani, S.Y. Wu, A.K. Sood, S. Hua, Advances and challenges of liposome assisted drug delivery, Front. Pharmacol. 6 (2015) 286.
[18] S.V. Talluri, G. Kuppusamy, V.V.S.R. Karri, S. Tummala, S.V. Madhunapantula, Lipid-based nanocarriers for breast cancer treatment–comprehensive review, Drug Deliv. 23 (4) (2016) 1291–1305.
[19] P. Mishra, B. Nayak, R. Dey, PEGylation in anti-cancer therapy: an overview, Asian J. Pharm. Sci. 11 (3) (2016) 337–348.
[20] M. Ghaferi, M.J. Asadollahzadeh, A. Akbarzadeh, H. Ebrahimi Shahmabadi, S.E. Alavi, Enhanced efficacy of PEGylated liposomal cisplatin: in vitro and in vivo evaluation, Int. J. Mol. Sci. 21 (2) (2020) 559.
[21] L.M. Kaminskas, V.M. McLeod, B.D. Kelly, G. Sberna, B.J. Boyd, M. Williamson, et al., A comparison of changes to doxorubicin pharmacokinetics, antitumor activity, and toxicity mediated by PEGylated dendrimer and PEGylated liposome drug delivery systems, Nanomed. Nanotechnol. Biol. Med. 8 (1) (2012) 103–111.
[22] M.B. Parsa, F. Tafvizi, V. Chaleshi, M. Ebadi, Preparation, characterization, and Co-delivery of cisplatin and doxorubicin-loaded liposomes to enhance anticancer Activities, Helion (2023).
[23] A. Jiménez-Escrig, F. Sánchez-Muniz, Dietary fibre from edible seaweeds: chemical structure, physicochemical properties and effects on cholesterol metabolism, Nutr. Res. (N.Y.) 20 (4) (2000) 585–598.
[24] P. Trucillo, R. Campardelli, E. Reverchon, Supercritical CO2 assisted liposomes formation: Optimization of the lipidic layer for an efficient hydrophilic drug loading, J. CO2 Util. 18 (2017) 181–188.
[25] K. Aramaki, Y. Watanabe, J. Takahashi, Y. Tsuji, A. Ogata, Y. Konno, Charge boosting effect of cholesterol on cationic liposomes, Colloids Surf. A Physicochem. Eng. Asp. 506 (2016) 732–738.
[26] P. Nakhaei, R. Margiana, D.O. Bokov, W.K. Abdelbasset, M.A. Jadidi Kouhbanani, R.S. Varma, et al., Liposomes: structure, biomedical applications, and stability parameters with emphasis on cholesterol, Front. Bioeng. Biotechnol. 9 (2021) 705886.
[27] A. Deniz, A. Sade, F. Severcan, D. Keskin, A. Tezcaner, S. Banerjee, Celecoxib-loaded liposomes: effect of cholesterol on encapsulation and in vitro release characteristics, Biosci. Rep. 30 (5) (2010) 365–373.
[28] H.-I. Chang, M.-K. Yeh, Clinical development of liposome-based drugs: formulation, characterization, and therapeutic efficacy, Int. J. Nanomed. (2012) 49–60.
[29] S. Shaker, A.R. Gardouh, M.M. Ghorab, Factors affecting liposomes particle size prepared by ethanol injection method, Research in pharmaceutical sciences 12 (5) (2017) 346.
[30] J. Tang, R. Kuai, W. Yuan, L. Drake, J.J. Moon, A. Schwendeman, Effect of size and pegylation of liposomes and peptide-based synthetic lipoproteins on tumor targeting, Nanomed. Nanotechnol. Biol. Med. 13 (6) (2017) 1869–1878.
[31] J.S. Suk, Q. Xu, N. Kim, J. Hanes, L.M. Ensign, PEGylation as a strategy for improving nanoparticle-based drug and gene delivery, Adv. Drug Deliv. Rev. 99 (2016) 28–51.
[32] N. Papp, J. Panicker, J. Rubino, G. Pais, A. Czechowicz, W.C. Prozialeck, et al., In vitro Nephrotoxicity and permeation of Vancomycin Hydrochloride loaded liposomes, Pharmaceutics 14 (6) (2022) 1153.
[33] M. de Silva, D.P. Siriwardena, C. Sandaruwan, G. Priyadarshana, V. Karunaratne, N. Kottegoda, Urea-silica nanohybrids with potential applications for slow and precise release of nitrogen, Mater. Lett. 272 (2020) 127839.
[34] Q. Rehman, M.S.H. Akash, M.F. Rasool, K. Rehman, Role of kinetic models in drug stability, Drug Stability and Chemical Kinetics (2020) 155–165.
[35] Y. Xu, B.W. Zhu, X. Li, Y.F. Li, X.M. Ye, J.N. Hu, Glycogen-based pH and redox sensitive nanoparticles with ginsenoside Rh2 for effective treatment of ulcerative colitis, Biomaterials 280 (2022) 121077.
[36] M. Najlah, A. Said Suliman, I. Tolaymat, S. Kurusamy, V. Kannappan, A.M. Elhissi, W. Wang, Development of injectable PEGylated liposome encapsulating disulfiram for colorectal cancer treatment, Pharmaceutics 11 (11) (2019) 610.
[37] M. Ghaferi, A. Raza, M. Koohi, W. Zahra, A. Akbarzadeh, H. Ebrahimi Shahmabadi, S.E. Alavi, Impact of PEGylated liposomal doxorubicin and carboplatin combination on glioblastoma, Pharmaceutics 14 (10) (2022) 2183.
[38] V.M. Steffes, Z. Zhang, S. MacDonald, J. Crowe, K.K. Ewert, B. Carragher, et al., PEGylation of paclitaxel-loaded cationic liposomes drives steric stabilization of bicelles and vesicles thereby enhancing delivery and cytotoxicity to human cancer cells, ACS Appl. Mater. Interfaces 12 (1) (2019) 151–162.
[39] M. Hoffmann, S. Gerlach, C. Hoffmann, N. Richter, N. Hersch, A. Csiszár, et al., PEGylation and folic-acid functionalization of cationic lipoplexes—improved nucleic acid transfer into cancer cells, Front. Bioeng. Biotechnol. 10 (2022) 1066887.
[40] R.X. He, X. Ye, R. Li, W. Chen, T. Ge, T.Q. Huang, X.J. Nie, H.J.T. Chen, D.Y. Peng, W.D. Chen, PEGylated niosomes-mediated drug delivery systems for Paeonol: preparation, pharmacokinetics studies and synergistic anti-tumor effects with 5-FU, J. Liposome Res. 27 (2) (2017) 161–170.
[41] B. Amiri, H. Ahmadvand, A. Farhadi, A. Najmafshar, M. Chiani, D. Norouzian, Delivery of vinblastine-containing niosomes results in potent in vitro/in vivo cytotoxicity on tumor cells, Drug Dev. Ind. Pharm. 44 (8) (2018) 1371–1376.
[42] E.A. Rustad, S. von Hofsten, R. Kumar, E.A. Lænsman, G. Berge, N. Škalko-Basnet, The pH-responsive liposomes—the effect of PEGylation on release kinetics and cellular uptake in glioblastoma cells, Pharmaceutics 14 (6) (2022) 1125.
[43] X. Wen, J. Li, D. Cai, L. Yue, Q. Wang, L. Zhou, et al., Anticancer efficacy of targeted shikonin liposomes modified with RGD in breast cancer cells, Molecules 23 (2) (2018) 268.
[44] C. Yang, H.Z. Liu, Z.X. Fu, Effects of PEG-liposomal oxaliplatin on apoptosis, and expression of Cyclin A and Cyclin D1 in colorectal cancer cells, Oncol. Rep. 28 (3) (2012) 1006–1012.
[45] I.T. Young, Proof without prejudice: use of the Kolmogorov-Smirnov test for the analysis of histograms from flow systems and other sources, J. Histochem. Cytochem. 25 (7) (1977) 935–941.
[46] S.K. Sriraman, V. Geraldo, E. Luther, A. Degterev, V. Torchilin, Cytotoxicity of PEGylated liposomes co-loaded with novel pro-apoptotic drug NCL-240 and the MEK inhibitor cobimetinib against colon carcinoma in vitro, J. Contr. Release 220 (2015) 160–168.
[47] D.A. Hsia, C.G. Tepper, M.R. Pochampalli, E.Y. Hsia, C. Izumiya, S.B. Huerta, et al., KDM8, a H3K36me2 histone demethylase that acts in the cyclin A1 coding region to regulate cancer cell proliferation, Proc. Natl. Acad. Sci. USA 107 (21) (2010) 9671–9676.
[48] J.N. Tung, C.C. Chiang, Y.Y. Tsai, Y.Y. Chou, K.T. Yeh, H. Lee, Y.W. Cheng, CyclinD1 protein expressed in pterygia is associated with β-catenin protein localization, Mol. Vis. 16 (2010) 2733.
[49] O.J. Prall, B. Sarcevic, E.A. Musgrove, C.W. Watts, R.L. Sutherland, Estrogen-induced activation of Cdk4 and Cdk2 during G1-S phase progression is accompanied by increased cyclin D1 expression and decreased cyclin-dependent kinase inhibitor association with cyclin E-Cdk2, J. Biol. Chem. 272 (16) (1997) 10882–10894.